Computer Methods and Programs in Biomedicine 175 (2019) 205–214

Contents lists available at ScienceDirect

Computer Methods and Programs in Biomedicine

journal homepage: www.elsevier.com/locate/cmpb

Automatic reconstruction method for high-contrast panoramic image from dental cone-beam CT data

Zhaoqiang Yun[a], Shuo Yang[b], Erliang Huang[c], Lei Zhao[a], Wei Yang[a], Qianjin Feng[a,*]

[a] Guangdong Provincial Key Laboratory of Medical Image Processing, School of Biomedical Engineering, Southern Medical University, Guangzhou, Guangdong, China
[b] Stomatological Hospital, Southern Medical University, Guangzhou, Guangdong, China
[c] Department of Medical Equipment, Guangzhou Women and Children's Medical Center, Guangzhou, Guangdong, China

ARTICLE INFO

Article history:
Received 11 March 2019
Revised 15 April 2019
Accepted 21 April 2019

Keywords:
Dental arch
Dental arch thickness
Cubic spline
Image enhancement
Panoramic image

ABSTRACT

Background and objective: Panoramic images reconstructed from dental cone beam CT (CBCT) data have been effectively used in dental clinics for disease diagnosis. Panoramic images generally have low contrast because excessive non-interest tissues participate in the reconstruction, which may affect the diagnosis. In this study, we developed a fully automatic reconstruction method to improve the global and detail contrast of panoramic images.

Methods: The proposed method consists of dental arch thickness detection, image synthesis, and image enhancement. First, the dental arch thickness is detected from an axial maximum intensity projection (MIP) image generated from the axial slices containing the teeth to reduce non-interest tissues in panoramic image reconstruction. Then, a new synthesis algorithm is proposed at image synthesis stage to reduce the effect of non-interest tissues on image contrast. Finally, an image enhancement algorithm is applied to the synthesized image to improve the detail contrast of the final panoramic image.

Results: A total of 129 real clinical dental CBCT data sets were used to test the proposed method. The panoramic images generated by three methods were subjectively scored by three experienced dentists who were blinded to the generated method. The evaluation of image contrast included the maxillary, mandible, teeth, and particular region (root canal, crown reconstruction, implants, and metal brackets). The overall image contrast score revealed that the proposed method scored the highest of 11.03 ± 2.46, followed by the ray sum and x-ray methods with corresponding scores of 6.4 ± 1.65 and 5.35 ± 1.56. The results of expert subjective scoring indicated that the image contrast of the panoramic image generated by the proposed method is higher than those of existing methods.

Conclusions: The proposed method provides a quick, effective and robust solution to improve the global and detail contrast of the panoramic image generated from dental CBCT data.

1. Introduction

In dentistry, CBCT [1] has become increasingly crucial in implant planning [2], abnormal teeth visualization, jaws evaluation, and bone augmentation image evaluation dental [3–5]. Panoramic images reconstructed from dental CBCT data serve an indispensable function in the post-processing of the oral image by providing an overview of oral and maxillofacial tissues for the dentist [6,7]. In general, the reconstruction of panoramic images can be divided into two steps. The first step is to extract an appropriate curve (i.e., dental arch) from dental CBCT data to express the arrangement of teeth in the jaw. In Fig. 1(e), the red curve is the dental arch, and the distance between the two blue curves is the dental arch thickness. The thickness of the dental arch determines the range of the region of interest that generates the panoramic image. The second step is to generate a panoramic image based on the first step. The original CBCT data between the two blue curves in Fig. 1(e) is unwrapped to obtain the curved multi-planar reconstruction (MPR) image set (Fig. 1(f)). The curved MPR image set cannot visualize the upper and lower dental arch information in one image. Therefore, a panoramic image (Fig. 1(g)) is generated from the curved MPR image set by using synthesis algorithms. Currently, the most widely used synthesis algorithm in the software system is the ray-sum or X-ray method [8–10], which uses parallel projection. The ray sum algorithm adds all values along the specified direction of the MPR image set to generate a panoramic image. The X-ray algorithm simulates real-world X-ray imaging, and the synthesis process follows the Beer-Lambert absorption-only model. Intensity

* Corresponding author at: School of Biomedical Engineering, Southern Medical University, 1023-1063 Shatai South Road, Baiyun District, 510515, Guangdong, China.
E-mail address: fengqj99@smu.edu.cn (Q. Feng).

https://doi.org/10.1016/j.cmpb.2019.04.024
0169-2607/

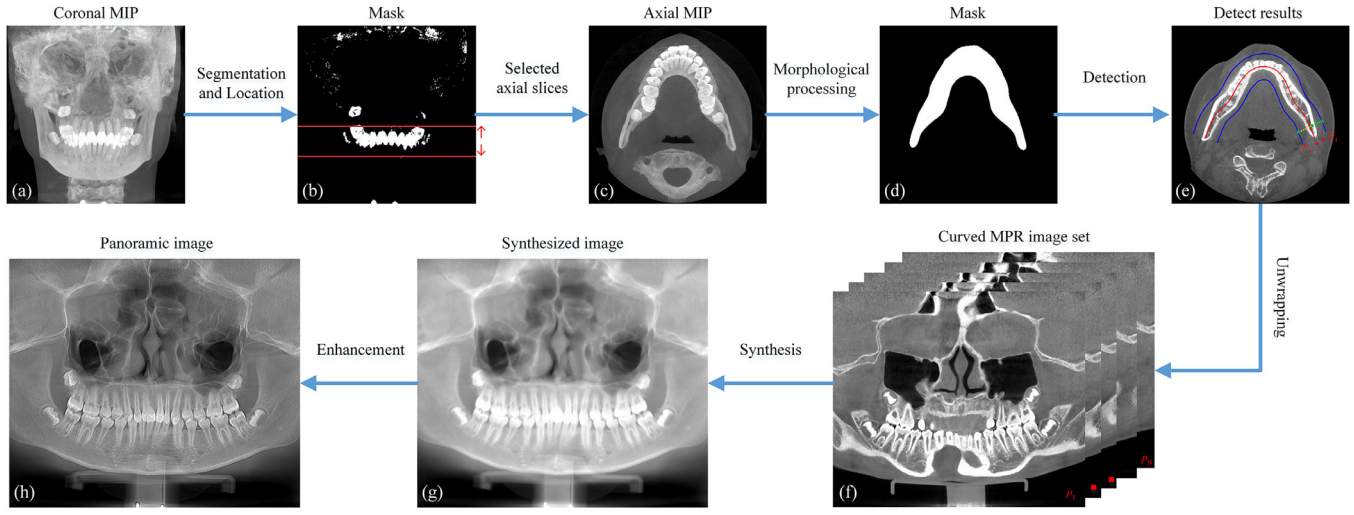

Fig. 1. Workflow of the proposed method.

attenuation for each ray is simulated depending on the medium's density but never reflected.

A single slice in the curved MPR image set has good contrast, but the contrast of the generated panoramic image is reduced. Low-contrast panoramic images affect the dentist's observation of the disease. The contrast of the panoramic image is mainly determined by two main factors: dental arch thickness and synthetic algorithm. The dental arch thickness determines the range of regions of interest (ROIs) contained around the dental arch that determines the number of slices in the curved MPR image set. The dental arch thickness is generally specified by the user. Manually specifying the thickness is inaccurate due to anatomical differences between patients. When the thickness is small, not all ROIs are included, resulting in incomplete information of the panoramic image. Conversely, including excessive non-interest tissues produces a blurred panoramic image. The optimal dental arch thickness should be the minimum value covering all ROIs. The other factor is the synthesis algorithm of the panoramic image. The MPR image set used to generate the panoramic image still has non-interest tissues, such as air and soft tissue, which significantly affect the synthesis results. Therefore, the accuracy of the dental arch thickness must be improved and the effect of non-interest tissues on the synthesis process must be suppressed to improve the contrast of panoramic images.

Related studies proposed different methods of dental arch detection, but few studies focused on improving the contrast of panoramic images. Automatic detection of the proper individual dental arch form for accurate orthodontic treatment is important [11]. The methods of dental arch detection can be categorized into two types: slice-based and MIP-based. The slice-based method detects the dental arch by processing the original CBCT slices [12,13]. First, an axial slice with the areas of mandible or maxilla is manually selected by the clinical expert/doctor. Second, a series of algorithms (including threshold segmentation, morphological operations, and curve fitting) is applied to the image to generate the dental arch. Finally, a curved MPR image set and a ray-sum panoramic image are generated. To solve the problem that requires the user to specify a slice manually, Amorim et al. [14] first applied a global threshold segmentation to all images. Then, the slice that contains the most pixels of white is chosen for dental arch detection. More recently, Papakosta et al. [15] proposed an automatic panoramic image reconstruction scheme from dental CT images, which is more robust for slice selection. The dental arch of each slice is identified and isolated from the original CBCT data. Then, the final dental arch is automatically selected from the dental arch group by comparison with the template polynomial obtained from the training set. The slice-based method detects the dental arch from an axial slice and does not maximize other CBCT information. It also has some other disadvantages, such as the need for users to specify the dental arch thickness manually and long calculation time resulting from the repetition of the same dental arch detection procedure for each axial slice. Unlike slice-based methods, MIP-based methods [16–18] generate the MIP image of the original CBCT data, and then the dental arch is detected by processing the MIP image. The typical process of MIP-based methods is to generate a MIP image of the specified range of axial slices. Then, a series of algorithms, including image segmentation and morphological operations, is applied to the MIP image to detect the dental arch. For special situations, such as the presence of occlusion fork in the mouth, the mandibular region is obtained from the MIP image of the dataset parallel to the Y-axis. Then, an axial MIP image is generated using the slices containing the mandible. MIP-based methods use the statistical properties of the original CBCT data; hence, the detected mask image contains information on the upper and lower jaws. Therefore, automatic detection of the dental arch thickness can be achieved based on the MIP image. Our method also utilizes the MIP image to detect the dental arch.

In the present study, we developed a fully automatic reconstruction method for high-contrast panoramic image from dental CBCT data. The proposed method consists of dental arch thickness detection, image synthesis, and image enhancement. The automatic detection of the dental arch thickness can effectively overcome the inaccuracy caused by the manual setting and effectively reduce the effect of non-interest tissues in the panoramic image reconstruction. Then, a new synthesis algorithm is proposed to effectively suppress non-interest tissues, such as air and soft tissue, to improve the overall contrast of panoramic images. To further improve the detail contrast of the panoramic image, we first propose to enhance the synthesized image based on the Gaussian filtering method to obtain the final panoramic image.

2. Materials and methods

2.1. Data acquisition

Clinical dental CBCT images of 129 patients were randomly collected by the Affiliated Stomatological Hospital of Southern Medical University, Guangzhou, China. The dataset was acquired using a NewTom VGi (QR s.r.l, Verona, Italy) scanner with the following parameters: 110 kVp, 3–8 mA (pulse mode). All patients were

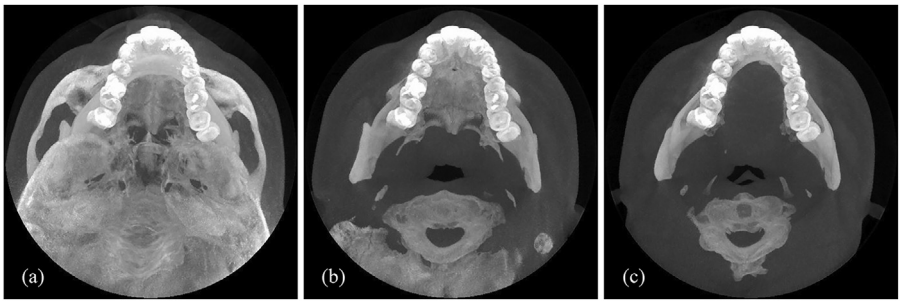

Fig. 2. MIP images generated by different ranges of the axial slices. (a) Full original CBCT data. (b) Axial slices containing upper and lower jaw. (c) Proposed method.

Table 1
Statistical results of the dataset.

Category	Age group						
	9–12	13–20	21–30	31–40	41–50	51–60	61–80
Metal bracket	0	4	3	0	0	0	0
Root canal	0	3	12	3	4	7	6
Crown restoration	0	0	4	5	5	8	7
Implant	0	0	1	2	1	4	2
Missing teeth	0	1	2	4	5	15	10
Total	4	16	33	16	13	28	19

anonymized at the time of export. The dataset was formatted in the DICOM standard as a series of 16-bit grayscale images (corresponding to individual CT slices). The size of all images was 512–512 pixels, with a 0.3–0.3 mm pixel size. In the dataset, the inter-slice distance was kept constant at 0.3 mm. The number of slices in each volume ranged from 322 to 541, depending on the patient.

The dataset included 70 females and 59 males aged 9–80 years. Among 129 patients, 16 patients had an occlusion fork in their mouth when scanning. Thus, the images of the 16 patients show that the upper and lower teeth are separated. Table 1 presents the statistical results of the dataset used in the experiment. Based on the impact on dental arch detection, the dataset is divided into six categories, namely metal bracket, root canal, crown restoration, implant, and missing teeth. Each row in Table 1 shows the distribution of the patient number of each category in different age groups, while the last rows illustrate the total number of patients in each age group. The age group represents different age ranges, a total of 7 age groups. The age group 9–12 had 4 patients. The images of these 4 patients show that the jaws have some tooth germs, which are mixed dentition. 7 patients in the 13–20 and 21–30 age groups were orthodontically treated with metal brackets. Root canal treatment and crown restoration had 35 and 29 patients, respectively. Among these patients, one had 7 teeth with root canal treatment, one had 11 teeth for crown restoration. 10 patients in the dataset underwent oral implant surgery, in which the implant material was titanium alloy. 37 patients had missing teeth, and one patient lost 11 teeth.

2.2. Proposed panoramic image reconstruction

An overview of the proposed method is shown in Fig. 1. The workflow of the proposed method consists of three steps. The first step is to detect the dental arch and the dental arch thickness from the input dental CBCT data (Fig. 1(e)). The second step is to obtain a curved MPR image set based on the detected dental arch and dental arch thickness and then to generate a synthesized image by using the synthesis algorithm (Fig. 1(g)). The last step is to apply an image enhancement algorithm to the synthesized image to obtain the final panoramic image (Fig. 1(h)).

2.2.1. Dental arch and dental arch thickness detection

MIP-based methods use an axial MIP image to detect the dental arch. The axial slice range used to generate the MIP image requires manual selection by the user. If the original CBCT data are used to generate the axial MIP image, excessive bone tissues are superimposed on the axial MIP image (Fig. 2(a)), which complicates the detection of the dental arch and the dental arch thickness. The MIP images generated by different ranges of the axial slice are present in Fig. 2. The axial slices containing the teeth must first be extracted from the original CBCT data to achieve a fully automated method and to improve the accuracy of dental arch thickness detection. Then, the axial MIP image generated by these axial slices is used for subsequent processing.

The enamel has the highest degree of calcification. Compared with other tissues, it has a higher absorption coefficient for X-rays and therefore has a higher intensity in image representation. This characteristic is more pronounced on MIP images. Therefore, the coronal MIP image (Fig. 3(a)) of the original CBCT data is generated first. The coronal MIP image is then passed through a threshold filter to obtain the mask image of the teeth. The threshold T used in threshold filtering is determined by the intensity histogram of the coronal MIP image. First, all peaks of the intensity histogram are detected. Then, a Gaussian curve fitting is estimated at the position of the peak with the largest gray value (Fig. 3(b)). The mean μ and the deviation σ are obtained by the Gaussian function. The threshold $T = \mu + 1.98\sigma$ for threshold filter.

After obtaining the mask image of teeth, the range of axial slices containing the teeth is determined. Depending on the diagnostic requirements, some patients need to place an occlusion fork in their mouths during scanning to separate the upper and lower jaw teeth. The illustration of the axial slice range detection in the two cases is shown in Fig. 3. The number of bright points in each row of the mask image is projected onto the Y-axis to generate a Y-histogram for determining the distribution of teeth on the mask image (Fig. 3(d)). Then, the highest peak is identified, and its width w is estimated by fitting a Gaussian curve (the mean μ_t and the deviation σ_t) to its shape. The width $w = 3 \times \sigma_t$ represents the enamel distribution on the MIP image. Let H indicate the number of peaks whose peak value is greater than half of the highest peak. If H is equal to 1, then no occlusion fork exists between the upper and lower teeth. The range of the axial slices containing the teeth is determined by the following formula:

$$\begin{aligned} A_s &= E_s - 2.5w \\ A_e &= E_s + 1.5w \end{aligned} \tag{1}$$

where E_s is the Y-axis position of the highest peak (the position of the solid line in Fig. 3(c)), A_s is the starting index of the axial slice, and A_e is the ending index of the axial slice.

$H \geq 2$, means an occlusion fork exists between the upper and lower teeth. The range of axial slices containing the teeth is

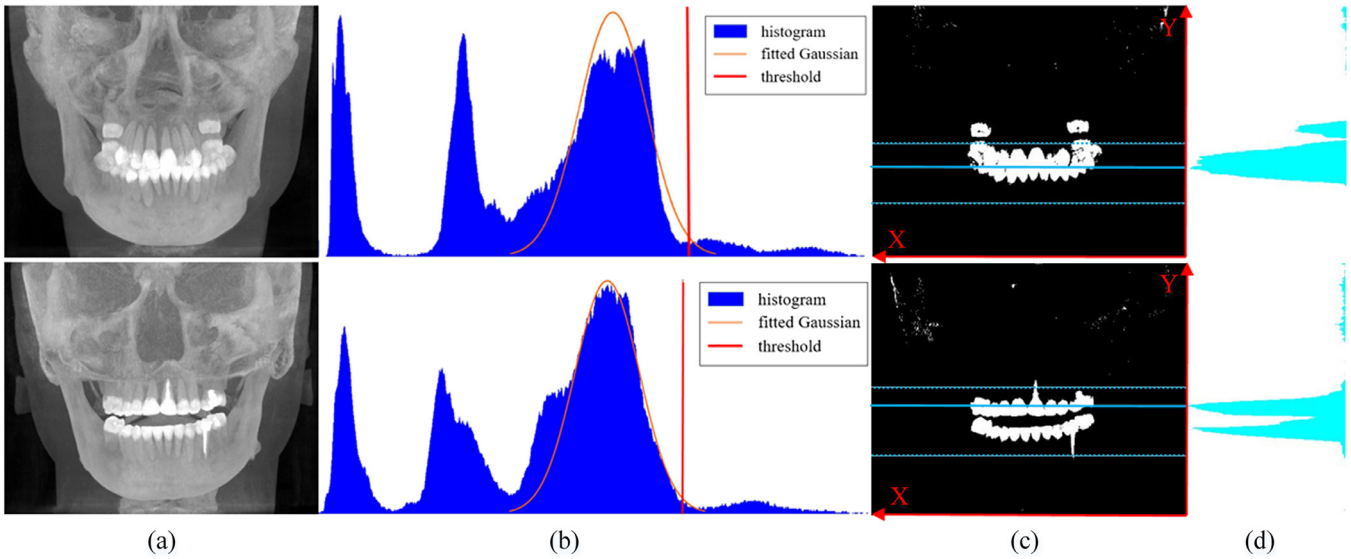

Fig. 3. Range of the axial slice containing the teeth. (a) Coronal MIP image. (b) Intensity histogram of the coronal MIP image. The vertical red line is the position of the threshold T. (c) Mask image of teeth. The two dashed lines are the range of detected axial slices used to generate the axial MIP image. (d) Y-axis histogram of the tooth mask image.

determined by the following formula:

$$A_s = E_b - 2.5w$$
$$A_e = E_t + 1.5w \tag{2}$$

where E_b and E_t are the Y-position of the two highest peaks of the Y-histogram, and $E_b < E_t$.

Then, an axial MIP image is generated using the axial slices between A_s and A_e, as shown in Fig. 1(c). The next step is to segment the axial MIP image for dental arch detection. The threshold is calculated in the same way as the coronal MIP image segmentation, and the axial MIP image is segmented by the threshold to obtain a mask image. In consideration that the contour of the jaws and teeth occupies the largest rectangular area in the mask image, the contour point sets of all connected regions are first extracted by the morphological operation, and then the area of each contour is calculated from the contour point set. The contour point set with the largest rectangular area is the contour of the jaws and teeth. Usually, the boundaries of the contour are very matte, and some burrs are present (upper left corner of Fig. 4). Therefore, a Gaussian smoothing is used to process the coordinates of the point set of the contour. The mask image is drawn using the smoothed point set (lower left corner of Fig. 4).

Finally, the mask image (Fig. 1(d)) is processed to detect the dental arch and the dental arch thickness (Fig. 1(e)). The first step is to process the mask image using the thinning algorithm [19–21] to obtain the skeleton. The skeleton performs the bifurcation detection and de-forking processing using morphological operations. The next step is to select control points at equal intervals on the skeleton. Studies [14] have shown that 11 control points can produce the smooth dental arch with enough approximation accuracy to the skeleton and low computational cost. The beginning and end of the skeleton are the first and last control points. The rest 9 control points are selected at equal intervals along the X-axis between the start and end control points. The final step is to generate a cubic spline curve from the 11 control points to represent the dental arch. An open source cubic splines library [22] is used to accomplish this task.

The dental arch thickness is estimated on the distance transform of the mask image (Fig. 1(d)). The distance transform is denoted by D. D is normalized to [0, 255] as follows:

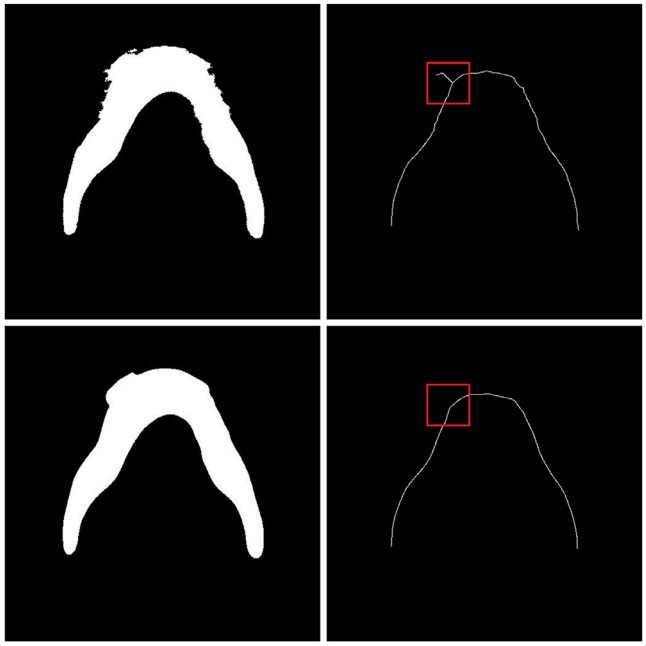

Fig. 4. Comparison of the mask image of the dental arch before and after Gaussian filtering and results of skeleton extraction.

$$D' = \frac{D}{D_{max}} * 255 \tag{3}$$

where D_{max} is the maximum value in D, and D' is the normalized distance transform. Let a pixel set $C = \{(x_k, y_k), k = 1,2,\ldots,K\}$ present the pixel in D' which values are greater than 245. For each pixel (x_k, y_k) in C, the perpendicular line l_k to the dental arch cross (x_k, y_k) is generated, and two intersection points between l_k and the boundaries of the mask image are determined. The distance between these two intersection points is denoted by L_k as a local thickness estimation. Then, the global dental arch thickness T_d is

estimated as:

$$T_d = \frac{1.2}{K} * \sum_{1}^{K} L_k \tag{4}$$

The parameters 245 in (3) and 1.2 in (4) in are empirically set to reduce the effect of noise and metal artifacts

2.2.2. Nonlinear synthesis algorithm

Before performing image synthesis, a curved MPR image set needs to be generated first. As shown in Fig. 1(f), the curved MPR image set is generated by unwrapping the pixels within the dental arch thickness centering on the dental arch (the red curve in the slice of Fig. 1(e)). The detailed process is described below. The first step is to perform an equal arc length sampling on the cubic spline curve to obtain a set of points on the curve. Equal arc length sampling is critical to improve the quality of panoramic images. Compared with equal pixel sampling, equal arc length sampling can effectively reduce jagged artifacts in the curved MPR images. Then, the lines perpendicular to the curve at sampling points are obtained. Centered on the sampling points, equidistant sampling is performed along the perpendicular lines on both sides of the curve. The number of sampling points on the perpendicular line is equal to the dental arch thickness. Finally, the pixel values sampled on the perpendicular lines are sequentially arranged into a curved MPR image set. The width and height of the curved MPR image set are the numbers of sampling points on the cubic spline curve and the number of axial slice of the original CBCT data. The thickness of the dental arch is the number of slices in the curved MPR image set.

The next step is to generate a synthesized image from the curved MPR image set. To suppress non-interest tissues, we propose a nonlinear synthesis algorithm in our framework. The synthesized image I_0 can be generated by the following formula:

$$I_0(i, j) = S * \log\left(\sum_{n=1}^{N} e^{P_n(i,j)/S}\right) \tag{5}$$

where i and j are pixel indexes of the synthesized image. The parameter S is a threshold of the tissue to be suppressed. To reduce the influence of non-interest tissues, such as air on the synthesized image, we set the threshold S to the intensity of the soft tissue. N is the number of images in the curved MPR image set. The value of N is equal to the dental arch thickness T_d. P represents an image in the curved MPR image set, and n represents the index of the curved MPR image.

2.2.3. Image enhancement

In general, the synthesized image generated from the MPR image set is a panoramic image, but the contrast of the panoramic image is unsatisfactory. The final step in our method proposes to enhance the synthesized image to improve the detail contrast of the panoramic image. The formula for the enhancement algorithm is as follows:

$$I = \alpha I_0 + (1 - \alpha)(I_0 - G(I_0)) \tag{6}$$

where α is the weight coefficient used to control the details of the enhancement. The value of α is set to 0.9. G represents a 2D Gaussian filtering function. The standard deviation of the Gaussian filtering function in the X and Y directions is 0.8. The Gaussian kernel size is 3×3. The selection of the parameters of the Gaussian filter will be detailed in the results section. I represents the final panoramic image.

3. Results

The proposed method was tested on a Dell machine (Intel(R) Core(TM) i5-3350P CPU 3.10 GHz, 12 GB RAM, running on a 64-bit Windows 10 system). The method was implemented in the Visual Studio 2015 with C++ and OpenCV library [23] and experimented using a wide variety of CBCT data sets. Panoramic images were successfully reconstructed from the tested dental CBCT dataset. The average running time of the proposed method is 3.2 s, the shortest running time is 2.4 s, and the maximum running time is 4.8 s, excluding the time of reading and saving the data set.

3.1. Dental arch and dental arch thickness detection results

The results of the dental arch and dental arch thickness detection of three CBCT data are presented in Fig. 5. The upper and lower teeth of Data3 are separate. The red curve is the detected dental arch. The distance between the two blue curves indicates the thickness of the dental arch. The thicknesses of the dental arch of the three CBCT data are 24.3, 29.4, and 28.2 mm. The first column shows the mandible, the second column shows the teeth of the mandible, and the third column shows the teeth of the maxilla. As shown in Fig. 5, the red curve approximately expresses the arrangement of the teeth in the jaw bone. All the jaw bones and teeth are included between the two blue curves. The blue curve on the underside of the red curve is close to the inner edge of the mandible. The blue curve above the red curve just fits the outer edge of the front tooth. The thickness of the dental arch is the minimum value that contains all ROIs.

3.2. Image enhancement

Fig. 6 shows the effect of enhancing the panoramic image with Gaussian filtering with different parameters. The different columns represent different Gaussian kernel sizes. The values of the kernel size from the first column to the last column are 3, 5, and 7. The different rows represent different standard deviations. The standard deviation in the X and Y directions is the same. The values of standard deviation from the first row to the last row are 0.6, 0.8, and 1.0. The change in kernel size exerts no significant effect on image contrast. As the standard equation increases, the details of the panoramic image improve. When the standard deviation is greater than 0.8, the enhancement effect is not apparent. Therefore, setting the kernel size and standard deviation of the Gaussian filter function to 3 and 0.8 is the optimal choice. Overall, the enhancement algorithm of the proposed method is not sensitive to the parameters.

3.3. Final panoramic image

The panoramic images generated by the typical six CBCT data are shown in Fig. 7. The six CBCT data are normal, mixed dentition, root canal, crown restoration, implant, and metal bracket. The six CBCT data cover all cases of the oral cavity. In these panoramic images, the incisor area and the molar area on both sides have a consistent brightness performance. The density and contrast among the enamel, dentine and pulp cavity are satisfactory. The maxillary sinus bottom edge is visible in the maxilla, and the mandibular canal and mental foramen are visible in the mandible. Fig. 7(a) shows a panoramic image of normal oral data generated with good global and detail contrast. For mixed dentition panoramic image (Fig. 7(b)), the dental follicle surrounding the tooth germ has a clear border. The panoramic image generated by the CBCT data of the filling and root canal treatment is shown in Fig. 7(c) and Fig. 7(e). The treatment area in the two panoramic images has a high contrast with the surrounding tissue, the shape is clear, and the layers are distinct. The panoramic image generated by the crown restoration CBCT data is shown in Fig. 7(d), with seven consecutive teeth treated. Since the restored crown has a high

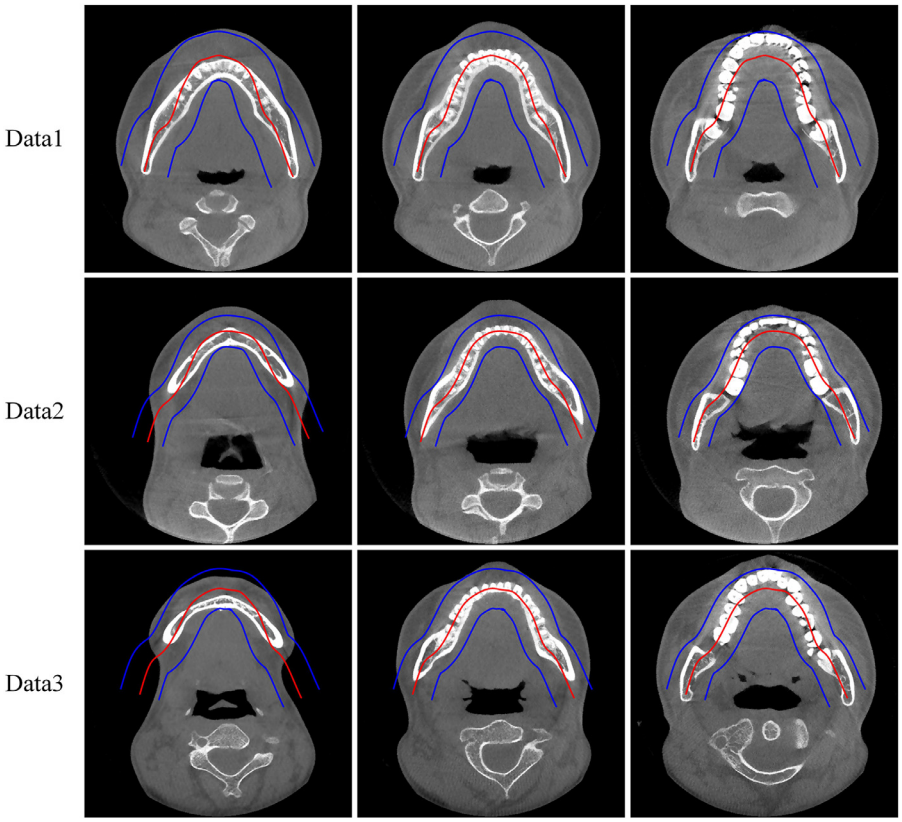

Fig. 5. Results of the dental arch and dental arch thickness detection in three CBCT data.

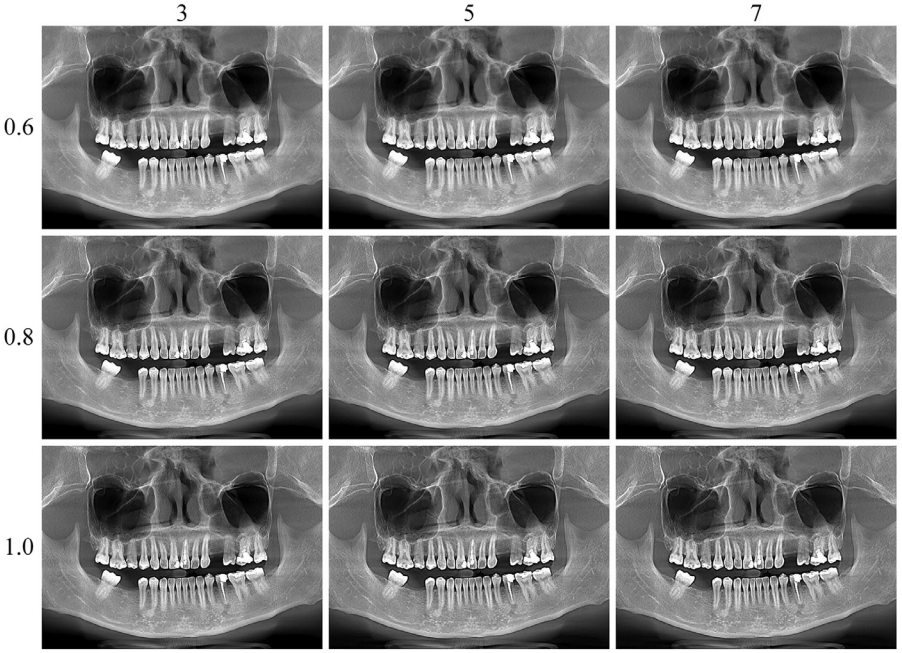

Fig. 6. Comparison of panoramic images under different enhancement parameters.

brightness, the overall image is displayed dark. Users can observe oral tissue information by adjusting window width and window level. Fig. 7(e) shows two implants on the mandible in the panoramic image, and the implant orientation and depth information of the implant can be observed. Finally, Fig. 7(f) shows a panoramic image of orthodontic treatment using a metal stent that has good contrast between the teeth and the metal stent so that the relationship between the tooth alignment and the metal stent can be easily observed.

3.4. Quantitative evaluation of the results

Qualitative assessment of panoramic image contrast was determined by three experienced dentists with at least 10 years of

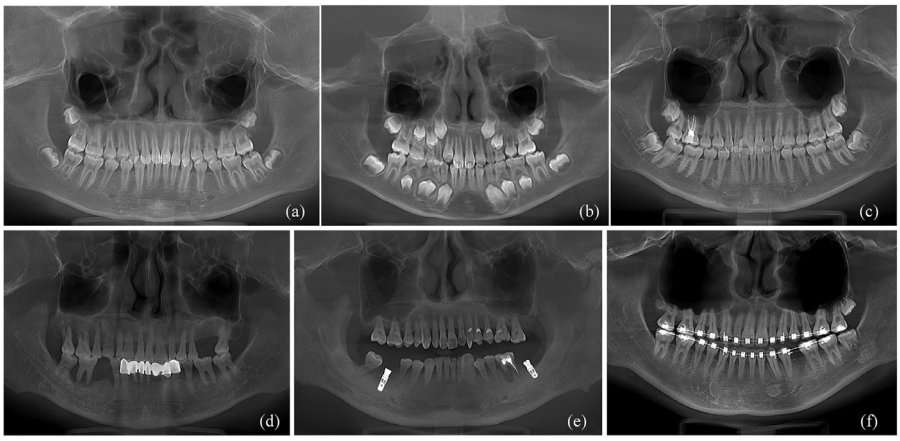

Fig. 7. Panoramic images generated by the proposed method.

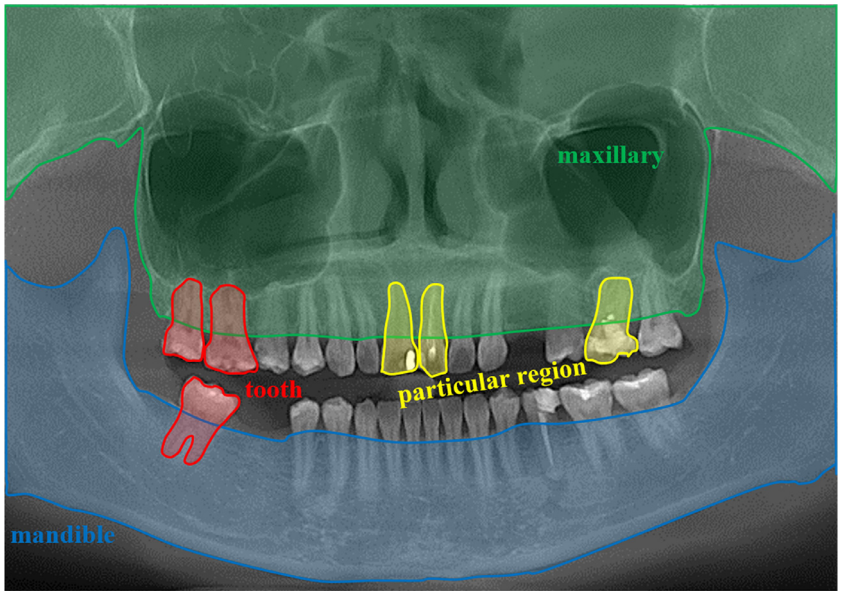

Fig. 8. Panoramic image was divided into four items for contrast assessment. The nomenclature for each item is defined as mandible, maxillary, teeth, and particular regions.

experience. The three reviewers were blinded to the method of generating panoramic image. Based on the dentist's experience in viewing panoramic images, the anatomical structures on the panoramic image were divided into four items: mandible, maxillary, teeth, and particular regions (Fig. 8). The particular regions represent treatment areas, such as root canals, crown restorations, implants, and metal brackets. Each item was evaluated individually. The score range for each item was 1–4 point, and the full score of the panoramic image was 16. If a particular region in a panoramic image was not scored by the dentist, the score of this particular region was set to the average value of the scores of the remaining regions. Although different aspects of evaluations have different score remarks, the numerical order for the grading scale remains unchanged with the higher score (3 or 4) representing better image contrast and the lower score (1 or 2) indicating poorer image contrast [24–26]. Details of the ordinal grading scale are presented in Table 2. The average score was then calculated from those four items to represent the contrast of each panoramic image.

The three dentists scored the panoramic images generated by the six methods according to the ordinal grading scale in Table 2. The evaluation results of the panoramic images are shown in Fig. 9. The overall image contrast score revealed that the proposed method has the highest score of 11.03 ± 2.46. In addition, the panoramic image of the image enhancement process has a significantly greater score than the non-enhanced panoramic image.

Table 2
Image contrast score descriptions.

Score	Description
1	The density and contrast between different tissues are poor. Significant structures are not visible and no diagnosis is possible.
2	The density and contrast between different tissues are unsatisfactory. The structure is visible
3	The density and contrast between different tissues are satisfactory. Un-uniform brightness of all tissues. Probably possible for diagnosis.
4	The density and contrast between different tissues are excellent. Uniform brightness of all teeth. Fine details are visualized with certain possible diagnosis.

4. Discussion

In the proposed framework, the dental arch and the dental arch thickness detection are based on the higher brightness of the teeth in the image, which is the keys to generating the final panoramic image. Two factors that affect the accuracy and success of dental arch and dental arch thickness detection are missing teeth and

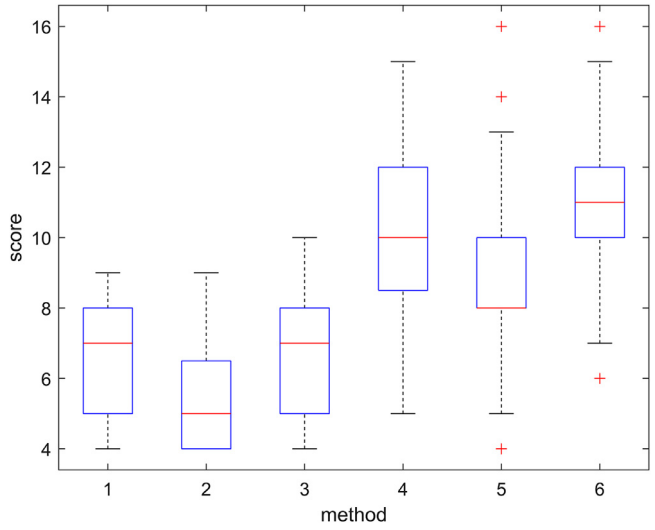

Fig. 9. Box plot showing the mean score of image contrast reported in the study. From methods 1 to 6 are ray-sum, x-ray, proposed synthesis algorithm, ray-sum + image enhancement, x-ray + image enhancement, and the proposed method. The image contrast score in the proposed method is the highest among all of the six groups.

metal artifacts. In general, missing some teeth does not affect the algorithm, and all missing tooth data in the test data sets successfully generate a panoramic image. In consideration of the limited data on missing teeth in the test data set, the detection algorithm requires more missing tooth data for testing.

The presence of metal artifacts is another critical factor influencing the detection of the dental arch and dental arch thickness. In CBCT images, the x-ray beam has lower mean kilovolt energy; thus the metal artifact is more pronounced. Severe metal artifacts can reduce the accuracy of the dental arch and dental arch thickness detection. Fig. 10(a) shows the results of the proposed method under the influence of severe metal artifacts. The red curve does not represent the arrangement of the teeth in the jaw bone, and the thickness of the dental arch is significantly too large. Both slice-based and MIP-based methods cannot overcome the effects of metal artifacts by post-processing. Metal artifacts can be suppressed or removed during CBCT reconstruction to improve the accuracy of the dental arch and dental arch thickness detection [27–29]. The metal artifact region in the CBCT data is automatically segmented, and then the projection image is processed by the back projection to the projection image. Finally, the projected image is processed to reconstruct the CBCT data. The above process requires precise reconstruction geometry and therefore needs to be done on the acquisition workstation.

The enhancement algorithm processing of synthesized images can effectively improve the contrast of panoramic images. The enhancement algorithm first performs Gaussian filtering on the image, which may result in halos artifacts. The halo artifacts occur when the area in the image is much brighter than the surrounding area. The halo artifacts cause low brightness at the edge of the high-brightness area. As shown in Fig. 10(b), the edges of the implant have a relatively dark outline after enhancement at the metal implant location in the panoramic image. The red rectangle is an enlarged display of the implant area. In recent years, some studies have estimated illumination images by correlation filtering and its improved algorithms [30–32], which can overcome some halo effects. However, for medical data with ultra-high brightness (such as fillings, root canals, crown restorations, implants, and metal brackets) reducing or avoiding halo artifacts is still a challenging task that needs to be solved in subsequent studies.

The dental arch thickness has a particular influence on the contrast of the panoramic image. Automatic dental arch thickness detection effectively reduces non-interest tissue involved in image synthesis. However, in the curved MPR image set, the jaw bone and teeth still only account for a small part of the image. As shown in Fig. 10(c), the yellow area is the jaw bone and tooth tissue, and

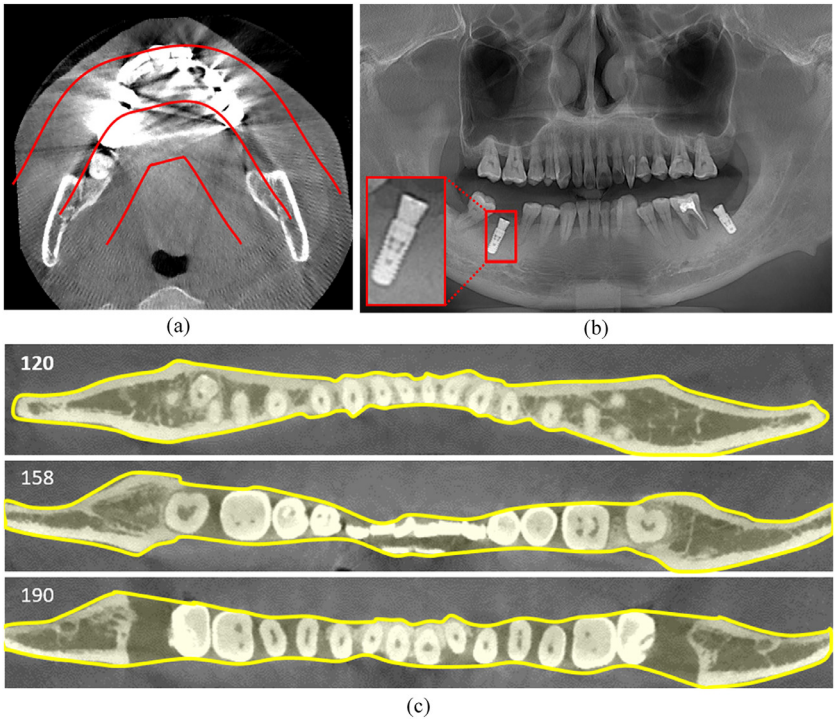

Fig. 10. (a) Dental arch thickness and dental arch detection results of severe metal artifact CBCT data. (b) Halo artifacts in panoramic image. (c) ROIs (yellow region) in different slices of the curved MPR image set.

the other is soft tissue. The synthesis of the panoramic image is performed along the vertical direction in the image. At different horizontal positions of the image, the percentage of the jaw and the teeth in the vertical direction shows a large change. To further reduce the effect of non-interest tissues on the image synthesis stage, future studies should explore non-uniform thickness detection methods of the dental arch. At different horizontal positions in Fig. 10(c), image synthesis is performed using different thicknesses to further reduce the effect of non-interest tissues participation.

Experimental results show that the synthesis algorithm improves the contrast of the panoramic image, but not at a significant level. Improving the contrast of panoramic images through synthetic algorithms requires further research. Previous studies focused on the detection of the dental arch, and the ray-sum or X-ray is mostly used to synthesize. The ray-sum and X-ray synthesis algorithms are direct volume rendering methods based on integrating volume data along the line of sight. In direct volume rendering, intensity is directly mapped to optical properties, such as color and opacity, which are then composited along the viewing direction into an image. This mapping is achieved using transfer functions. For panoramic images, a transfer function can be used to convert the intensity to absorption coefficients that increase with intensity. For different tissues, the absorption coefficient is generated using different methods to suppress or strengthen different tissues. In our future work, we will explore transfer function generation methods for panoramic image synthesis to improve the quality of panoramic images further.

5. Conclusion

Automatic generation of panoramic images from dental CBCT data is an essential function in image post-processing. In this study, an automatic method is proposed for high-contrast panoramic image reconstruction from dental CBCT data. The method is an effective and robust solution to improve the global and detail contrast of panoramic images. The proposed method mainly includes three parts: dental arch thickness detection, synthesis algorithm, and image enhancement algorithm. The thickness detection of the dental arch can effectively overcome the inaccuracy of the manual setting and reduce non-interest tissues in panoramic image reconstruction. The new synthesis algorithm suppresses or strengthens different tissues during the curved MPR image set synthesis to improve the contrast of the resulting image. Finally, the enhancement algorithm is applied to improve the detail contrast of the panoramic image. The thickness detection of the dental arch proposed in the method can be applied to the dental arch detection on MIP-based methods. The synthesis algorithm and image enhancement algorithms proposed in the method can be applied to manual or automatic panoramic image reconstruction alone to improve the contrast of panoramic images.

Funding

This study was supported by the National Key R&D Program of China (grant number 2017YFC0112801); Major Program of National Natural Science Foundation of China (grant number U15012561016942); The Science and Technology Planning Project of Guangdong Province, China (grant number 2013B090600139 and 2015B010131011); and Guangdong Provincial Key Laboratory of Medical Image Processing (no. 2014B030301042).

Conflicts of interest

The authors declare that there is no conflict of interest regarding the publication of this paper.

References

[1] W.C. Scarfe, C. Angelopoulos, Maxillofacial Cone Beam Computed Tomography: Principles, Techniques and Clinical Applications, Springer, 2018, doi:10.1007/978-3-319-62061-9.
[2] G. Fokas, V.M. Vaughn, W.C. Scarfe, M. Bornstein, Accuracy of linear measurements on CBCT images related to presurgical implant treatment planning: a systematic review, Clin. Oral. Implants Res. 29 (2018) 393–415, doi:10.1111/clr.13142.
[3] V. Manavella, F. Romano, F. Garrone, M. Terzini, C. Bignardi, M. Aimetti, A novel image processing technique for three-dimensional volumetric analysis of severely resorbed alveolar sockets with cone beam computed tomography, Minerva Stomatol. 66 (2017) 81–90, doi:10.23736/S0026-4970.17.04029-8.
[4] M. Aimetti, V. Manavella, L. Corano, E. Ercoli, C. Bignardi, F. Romano, Three-dimensional analysis of bone remodeling following ridge augmentation of compromised extraction sockets in periodontitis patients: a randomized controlled study, Clin. Oral Implants Res. 29 (2) (2018) 202–214, doi:10.1111/clr.13099.
[5] V. Manavella, F. Romano, L. Corano, C. Bignardi, M. Aimetti, Three-dimensional volumetric changes in severely resorbed alveolar sockets after ridge augmentation with bovine-derived xenograft and resorbable barrier: a preliminary study on CBCT imaging, Int. J. Oral. Maxillofac. Implants 33 (2018) (2018) 373–382, doi:10.11607/jomi.5684.
[6] M.E. Çiftçi, A.M. Aktan, Ö. İşman, E. Yıldırım, Relationship between CBCT and panoramic images of the morphology and angulation of the posterior mandibular jaw bone, Surg. Radiol. Anat. 38 (2016) 313–320, doi:10.1007/s00276-015-1553-1.
[7] H. Fujimoto, T. Hayashi, M. Iino, A novel method for landmark-based personal identification on panoramic dental radiographic and computed tomographic images, J. Forensic Radiol. Imaging 7 (2016) 21–27, doi:10.1007/s00276-015-1553-1.
[8] P. Henzler, V. Rasche, T. Ropinski, T. Ritschel, Single-image tomography: 3D volumes from 2D cranial X-rays, Comput. Graph. Forum (2018) 377–388, doi:10.1111/cgf.13369.
[9] S. Suzuki, K. Ichikawa, S. Tamaki, Image quality and clinical usefulness of ray-summation image reconstructed from ct data, compared with digital radiography, Jap. J. Radiol. Tech. 73 (2017) 372–381, doi:10.6009/jjrt.2017_JSRT_73.5.372.
[10] M.A. Westenberg, J.B. Roerdink, X-ray volume rendering by hierarchical wavelet splatting, ICPR IEEE 3 (2000) 159–162, doi:10.1109/ICPR.2000.903509.
[11] M. Bae, J. Park, N. Kim, Semi-automatic and robust determination of dental arch form in dental cone-beam CT with B-spline approximation, Comput. Methods Programs Biomed. 172 (2019) 95–101, doi:10.1016/j.cmpb.2019.02.013.
[12] T. Chanwimaluang, S. Sotthivirat, W. Sinthupinyo, Automated dental arch detection using computed tomography images, in: Proc. of the 9th International conference on Signal Processing, 2008, pp. 737–740, doi:10.1109/ICOSP.2008.4697235.
[13] V. Sa-ing, K. Wangkaoom, S.S. Thongvigitmanee, Automatic dental arch detection and panoramic image synthesis from CT images, in: 35th Annual International Conference of the IEEE EMBS, 2013, pp. 6099–6102, doi:10.1109/EMBC.2013.6610944.
[14] P. Amorim, T.D. Moraes, J.D. Silva, H. Pedrini, R. Ruben, Automatic reconstruction of dental CT images using optimization, Biodental Eng. 57 (2014), doi:10.1201/b17071-12.
[15] T.K. Papakosta, A.D. Savva, T.L. Economopoulos, G.K. Matsopoulos, H. Gröhndal, An automatic panoramic image reconstruction scheme from dental computed tomography images, Dentomaxillofacial Radiol. 46 (2017) 20160225, doi:10.1259/dmfr.20160225.
[16] H. Akhoondali, R.A. Zoroofi, G. Shirani, Fully automatic extraction of panoramic dental images from CT-scan volumetric data of the head, J. Appl. Sci. 9 (2009) 2106–2114, doi:10.3923/jas.2009.2106.2114.
[17] H. Bing, C. Liang, C. Zhen, P. Fang, L. Deyu, L. Shuyu, F. Yubo, An automatic method of synthesizing panoramic radiograph by unwrapping dental CT image, international conference on mechatronic science, Electric Eng. Comput. (2011) 1094–1096, doi:10.1109/MEC.2011.6025657.
[18] T. Luo, C. Shi, X. Zhao, Y. Zhao, J. Xu, Automatic synthesis of panoramic radiographs from dental cone beam computed tomography data, PLoS One 11 (2016) e0156976, doi:10.1371/journal.pone.0156976.
[19] R.W. Hall, Fast parallel thinning algorithms: parallel speed and connectivity preservation, Commun ACM 32 (1989) 124–131, doi:10.1145/63238.63248.
[20] P. Wang, Y. Zhang, A fast serial and parallel thinning algorithm, Cybernet Syst (1986) 909–915, doi:10.1007/978-94-009-4634-7_117.
[21] T.Y. Zhang, C.Y. Suen, A fast parallel algorithm for thinning digital patterns, Commun ACM 27 (1984) 236–239, doi:10.1145/357994.358023.
[22] T. Kluge, Cubic Spline Interpolation in C++, 2014 https://kluge.in-chemnitz.de/opensource/spline/.
[23] OpenCV, 2018, https://opencv.org/.
[24] C. Gamache, J.D. English, A. SalasLopez, J. Rong, S. Akyalcin, Assessment of image quality in maxillofacial cone-beam computed tomography imaging, Semin Orthod. 21 (4) (2015) 248–253, doi:10.1053/j.sodo.2015.07.002.
[25] F. Gijbels, A.D Meyer, C.B. Serhal, C.V. Bossche, J. Declerck, M. Persoons, R. Jacobs, The subjective image quality of direct digital and conventional panoramic radiography, Clin. Oral. Invest. 4 (2000) 162–167, doi:10.1007/s007840000059.
[26] Z. Wang, A.C. Bovik, H.R. Sheikh, E.P. Simoncelli, Image quality assessment: from error visibility to structural similarity, IEEE T Image Process. 13 (2004) 600–612, doi:10.1109/TIP.2003.819861.

[27] F.E. Boas, D. Fleischmann, CT artifacts: causes and reduction techniques, Imaging Med. 4 (2012) 229–240, doi:10.2217/iim.12.13.
[28] I. Ibraheem, Reduction of artifacts in dental cone beam CT images to improve the three dimensional image reconstruction, J. Biomed. Sci. Eng. 5 (2012) 409–415, doi:10.4236/jbise.2012.58052.
[29] C. Nardi, C. Borri, F. Regini, L. Calistri, A. Castellani, C. Lorini, S. Colagrande, Metal and motion artifacts by cone beam computed tomography (CBCT) in dental and maxillofacial study, Radiol. Med. 120 (7) (2015) 618–626, doi:10.1007/s11547-015-0496-2.
[30] M.S. Lee, C.H. Park, M.G. Kang, Edge enhancement algorithm for low-dose X-ray fluoroscopic imaging, Comput. Methods Programs Biomed. 152 (2017) 45–52, doi:10.1016/j.cmpb.2017.09.010.
[31] L. Xiong, H. Li, L. Xu, An enhancement method for color retinal images based on image formation model, Comput. Methods Programs. Biomed. 143 (2017) 137–150, doi:10.1016/j.cmpb.2017.02.026.
[32] C. Zhao, Z. Wang, H. Li, X. Wu, S. Qiao, J. Sun, A new approach for medical image enhancement based on luminance-level modulation and gradient modulation, Biomed. Signal Process. Control 48 (2019) 189–196, doi:10.1016/j.bspc.2018.10.008.